Eurasian Journal of Physics and Functional Materials

2023, 7(2), 79-90

Non-destructive structural studies of ceramic fragments of ancient tribes of Kazakhstan

A.Zh. Zhomartova[*,1,2,3], B.A. Bakirov[1,4],
S.E. Kichanov[1], R.S. Zhumatayev[5],
A.T. Toleubayev[5], S. Shakenov[5], D.P. Kozlenko[1]

[1]Joint Institute for Nuclear Research, Dubna, Russia

[2]L.N. Gumilyov Eurasian National University, Astana, Kazakhstan

[3]Institute of Nuclear Physics, Ministry of Energy of the Republic of Kazakhstan, Almaty, Kazakhstan

[4] Kazan Federal University, Kazan, Republic of Tatarstan, Russia

[5]Al-Farabi Kazakh National University, Almaty, Kazakhstan

E-mail: zhomartova@jinr.ru

DOI: **10.32523/ejpfm.2023070201**
Received: 17.06.2023 - after revision

The phase composition of several fragments of the ancient ceramic of the early medieval settlement of Asusay and burial ground Eleke Sazy in the modern Republic of Kazakhstan has been studied using neutron diffraction and Raman spectroscopy. The quartz, calcite, and feldspar minerals are dominant phases in the studied ceramic fragments. The fractions of those phases were obtained. The spatial arrangement of inner components inside volumes of fragments was determined using neutron tomography. The pores in the ceramic fragments were segmented, and the porosity for each sample was obtained. The phase composition and internal pores are discussed within the framework of the structural indicators of local clay sources and features of ancient pottery technologies.

Keywords: neutron tomography; neutron diffraction; Raman spectroscopy; ancient ceramics; phase analysis.

Introduction

Among ancient archaeological artifacts, the ceramic materials as entirely preserved objects or those fragments often play a key role in determining the location

of a pottery workshop, specifics of the pottery manufacture method, and the trade or expansion ways of cultural groups or historical communities [1-3]. Despite the availability and spread of pottery fragments, the ancient ceramics are complex archeological materials with unique structural prints, including definite crystalline or amorphous phases, the unpredictable spatial distribution of components, doubt concerning the matter of glaze or pigments of the decoration layers [4]. Also, the ancient pottery materials are useful model objects for studying internal degradation over time, the propagation of cracks and voids in the thickness of the pottery items, and the effects of annealing or reinforcement additives on the physic-chemical properties of ceramic products such as tableware, utensils, religious objects, decorative items, etc. Recently, non-destructive neutron methods have shown wide possibilities for the structural study of cultural heritage objects [5, 6]. Neutron methods are characterised by higher penetration into the thickness of metal and ceramic objects in comparison with X-ray radiation methods. On the other hand, ancient communities and nationalities that lived on the territory of modern Kazakhstan, represent a unique mixture of Turkic and Saka cultural groups [7]. It is known that the tribes were well-versed in nomadic cattle breeding as well as in settled agriculture. This and the local natural features of the region leave their mark on the style and technology of producing ceramic products among the ancient tribes of Kazakhstan. Several archeological expeditions have explored one of the branches of the Silk Road between the Zhongar (Zhetysu) of Alatau and the Tarbagatay ridge [7, 8]. One of the oldest medieval settlements around Lake Alakol is the Asusay settlement, located southwest of the village of Akshi in the Alakol district of the Almaty region [7]. One of the interesting archeological finds are remains of the old irrigation systems around the settlement, which consist of canals diverted from the river, and fragments of stone mills of various sizes that were discovered in the area of the settlement [9]. Large numbers of ceramic fragments of the simple dishes without glaze used in everyday life were found during the archeological excavations in the trade zone of the Asusay settlement. For comparison, we used several ceramic fragments found in the burial ground of Eleke Sazy. Unique burial complexes from the Early Saka (VII century BC) to the Late Turkic (VIII century AD) periods were discovered here. The complex locates in the eastern Kazakhstan at an altitude of 1500 meters above sea level in the Tarbagatay Mountains.

To research the structural features of several ceramic fragments from different historical complexes on the territory of modern Kazakhstan, we prepared detailed structural studies using neutron tomography, neutron diffraction, and Raman spectroscopy.

Materials and methods

Sample description

For neutron structural studies, we have chosen two groups of ceramic fragments. There are archeological samples from the Asusay settlement and ceramic frag-

ments from the Eleke Sazy complex. These ceramic samples represent the ancient population of southern and eastern parts of modern Kazakhstan.

The photos of the studied fragments are shown in Figure 1. The samples S_1, S_2, and S_3 were discovered during archeological excavations of the medieval settlement of Asusay, located on the shore of Lake Alakol in the Almaty region of Kazakhstan. The samples S_4, S_5, S_6, and S_7 were found in the grave complex of Eleke Sazy. The S_4 and S_5 samples were found in mound No. 7; S_6 and S_7 in mound No. 20, located on the right side of the Kargyba River in Tarbagatay district of the East Kazakhstan region. The pottery clay of the studied samples is well-prepared, dense, and uniform in the fracture of the shard. The inner and outer surfaces are red. The same color in the slice indirectly indicates a uniform annealing temperature. An ornament prepared by the immersion of a solid substance is visible.

Figure 1. The photos of the ceramic fragments and its sample labels. The scale bar is shown.

The design futures of ornament indicate that fragments relate to similar archeological items from the medieval Kazakh settlement of Taraz [10], which can tentatively relate the studied fragments to the medieval period of the XI-XII century AD.

Raman Spectroscopy

The primary analysis of the phase composition of the ceramic samples was performed using Raman spectroscopy. The experiments were prepared using the LabRam HR spectrometer (Horiba Gr, France) with a Leica M165 microscope equipped with a He-Ne laser with an excitation wavelength of 633 nm, a x20 objective, an 1800 grating, and a confocal hole of 200 μm. Raman spectra were recorded at different local points on the surface of the studied fragments. All spectra were measured in the range of $50-2000$ cm^{-1}, and the exposition for each point was 5 min. The tentative identification of the Raman spectra was performed by comparing the obtained spectra with the reference data [11].

Neutron diffraction

The phase composition of the ceramic fragments was analyzed by neutron diffraction using the DN-6 diffractometer [12] at the IBR-2 high-flux pulsed reactor of the Frank Laboratory of Neutron Physics, JINR, Dubna, Russia. The resolution of the diffractometer was $\triangle$ d / d = 0.025 for scattering angles $2\theta = 90^{\circ}$. The exposure time for each sample was 20 minutes. The neutron diffraction patterns were fitted by the Rietveld method using the Fullprof software [13].

Neutron tomography

The inner structure of the ceramic fragments was investigated using the neutron radiography and tomography facility [14, 15] located at the IBR-2 high-flux pulsed reactor. The neutron images were collected using the detector system based on the scintillator ^{6}LiF/ZnS screen and the high-sensitivity camera with the Hamamatsu CCD chip [16]. For the tomography reconstruction [17], the 360 neutron radiographic images for the different angular positions of the sample relative to the neutron beam direction were collected. The rotation step of the goniometer in the tomography experiments was 0.5°. The exposition time for one radiography projection was 20 s. The imaging data were corrected by the dark current image and normalized to the image of the incident neutron beam using the ImageJ software [18]. The scattering and absorption losses account for the attenuation of the neutron beam inside the material [17]. The reconstruction of three-dimensional (3D) data of the studied fragments was performed by the SYRMEP Tomo Project application [19]. The reconstructed 3D volume data consisted of voxels, which coded the spatial distribution of the neutron attenuation coefficients at each point of a sample. The visualization and analysis of the reconstructed 3D models were performed using VGStudio MAX software (Volume Graphics, Heidelberg, Germany).

Results and discussion

Raman spectroscopy

The examples of Raman spectra, which corresponded to different composite phases of the ceramic fragments, are shown in Figure 2. In addition to the typical phases such as quartz, feldspar, and carbon, it was also possible to identify magnetite, corundum, and anatase. The quartz phase was detected by characteristic lines at 126, 200, 356, and 463 cm^{-1} [20]. Several Raman lines (sample S_2) at 290, 478, and 508 cm^{-1} were attributed to the feldspar phase [21]. The most intense Raman lines at 1368 and 1398 cm^{-1} of the samples from the settlement of Asusay can be attributed to the corundum phase [22]. The Raman line at 144 cm^{-1} corresponds to the anatase phase. The anatase phase is represented by rounded grains up to 10 microns in size (Figure 2). In comparison with the ceramic samples from the Eleke Sazy place, the magnetite phase with the characterised line at 670 cm^{-1} [22] was detected for the S_1, S_2, and S_3

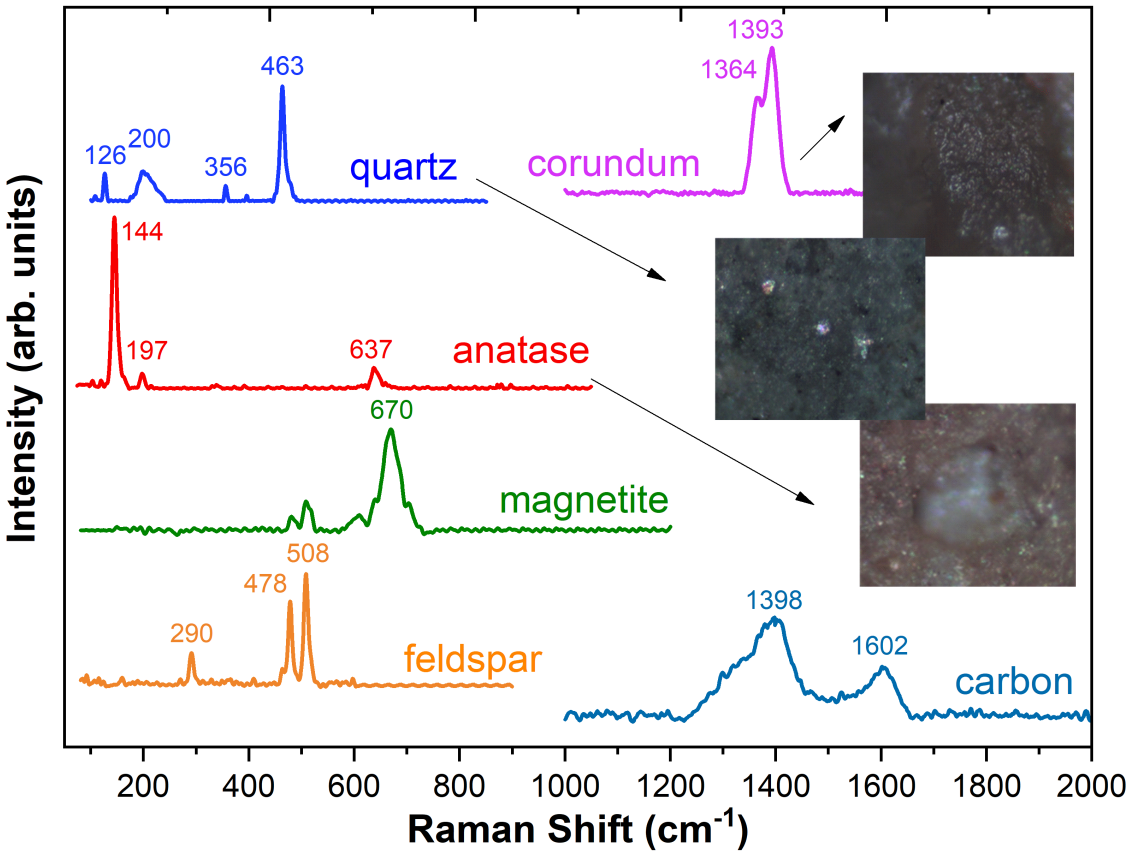

Figure 2. Characteristic Raman spectra were obtained on the surface of the ceramic fragments. The mineral is labeled. The enlarged microscopic images of the correspondingly measured local areas are presented.

samples only. These samples are from the Asusay settlement. The carbon phase was observed in several studied samples. We assumed that the presence of soot in ceramic fragments was highly possible. It can be explained that some organic matter (bark, grass, straw, wool, or manure) [23, 24] can be admixed with clay for the reinforcement process. The results of the analysis of Raman spectroscopy data are presented in Table 1.

The characteristic Raman lines for the feldspar phase are a duplet in a range 470-510 cm $^{-1}$ at the Raman spectra. The relative difference in the peak positions of the duplet is indicated by the mineral composition of clay [21]. The relative positions of the feldspar duplet for the studied samples are shown in Figure 3. Interestingly, the S_2 and S_4 samples have slightly different duplet position compared to the other samples. We can estimate that the clay for ceramic fragments of S_2 and S_4 is characterized by a high content (up to 80 %) of albite, while other samples contain orthoclase-rich minerals [21].

Table 1.
The observed mineral phases for the ceramic fragments according to Raman spectroscopy data. The names of the minerals and their corresponding Raman lines are presented. The line intensities are denoted by the s-small, m-medium, and w-weak labels. Most intense Raman lines are marked in bold.

Sample	Observed Phases by Raman spectroscopy. The positions of Raman peaks in cm^{-1}
S_1	Quartz [128(m), 205(m), **464**(s)], Anatase [**143**(s), 197(w), 639(m)], Magnetite [**670**(s)], Feldspar [292(m), **478**(s), **508**(s)]
S_2	Quartz [125(m), 201(m), 354(w), **462**(s)], Anatase [**143**(s), 638(m)], Magnetite [**683**(s)], Feldspar [290(m), **478**(s), **508**(s)], Corundum [**1365**(s), **1394**(s)], Carbon [**1376**(s), 1604(m)]
S_3	Quartz [126(m), 200(m), 356(w),], Anatase [**145**(s), 639(m)], Magnetite [**670**(s)], Feldspar [**509**(s)], Corundum [**1363**(s), **1393**(s)], Carbon [**1398**(s), 1602(m)]
S_4	Quartz [128(m), 206(m), 355(w), 402(w), **464**(s)], Anatase [**145**(s), 198(w), 635(m)], Feldspar [158(m), 283(m), 475(m), **513**(s)]
S_5	Quartz [128(m), 205(m), 355(w), **464**(s)], Anatase [**144**(s), 637(m)], Feldspar [290(m), **478**(s), **509**(s)]
S_6	Quartz [206(m), **464**(s)], Anatase [**145**(s), 198(w), 511(w), 638(m)], Feldspar [**476**(s),**514**(s)]
S_7	Quartz [128(m), 207(m), 356(w), **465**(s)], Anatase [**143**(s)], Feldspar [**511**(s)]

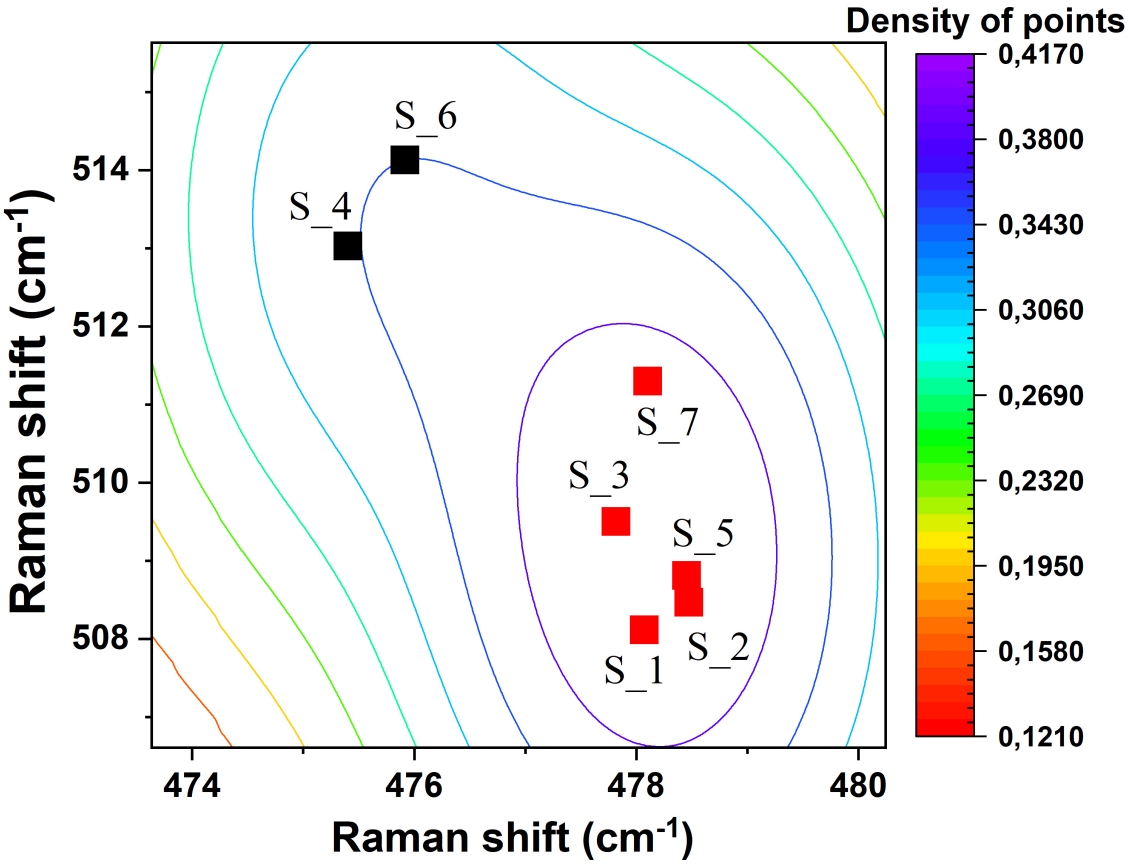

Figure 3. The positions of doublet assigned to the feldspar phase of the clay material. The data clustering was estimated by the Kernel Smooth Distribution approximation [25]. The obtained density of points as a result of the approximation is presented by a color bar as well as the contour lines.

Neutron diffraction

The examples of neutron diffraction patterns of selected ceramic samples are shown in Figure 4.

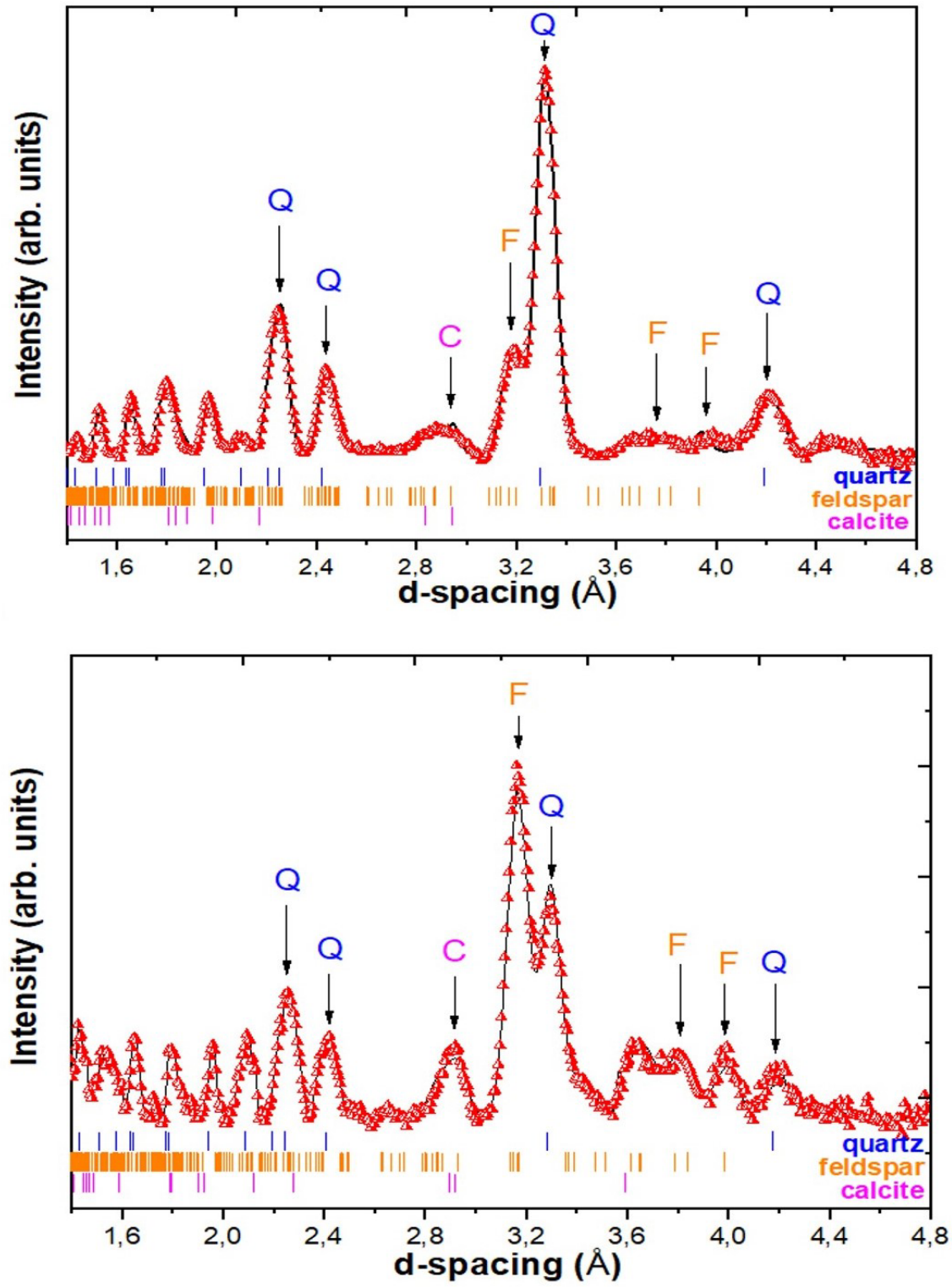

Figure 4. The neutron patterns of the S_1 and S_6 ceramic fragments. The experimental points and the calculated profile by the Rietveld method are presented. The calculated positions of the Bragg peaks corresponding to the dominant phases (quartz, feldspar, and calcite) are labeled. The diffraction peaks related to the quartz (Q), calcite (C), and feldspar (F) phases are marked.

As expected, quartz and feldspar are the dominant phases of the ceramic fragments [26]. The quartz has a crystal structure with the trigonal space group $P3_121$ [27]. The average lattice parameters of the quartz phase for the ceramic samples are a = 4,908(5) Å and c = 5,414(4) Å [28]. The crystal structure of feldspar is described by a triclinic symmetry $C\bar{1}$ with average lattice parameters a = 8.23(6), b = 12.78(5), c = 7.08(1), $\alpha = 91.17(3)^\circ$, $\beta = 115.54(2)^\circ$, $\gamma = 90.14(1)^\circ$. There are additional weak diffraction peaks corresponding to the Mg-calcite phase. The crystal structure of the calcite phase is rhombohedral with the $R\bar{3}c$ space group; the calculated average lattice parameters are a = 4.916(2) Å and c = 16.824(3) Å. The presence of the calcite phase in the clay mass can indicate indirectly the presence of limestone [29].

The phase fractions were calculated from neutron diffraction data. The relative volume content of the dominant mineral phases in the ceramic fragments was calculated using the Rietveld method (Figure 5).

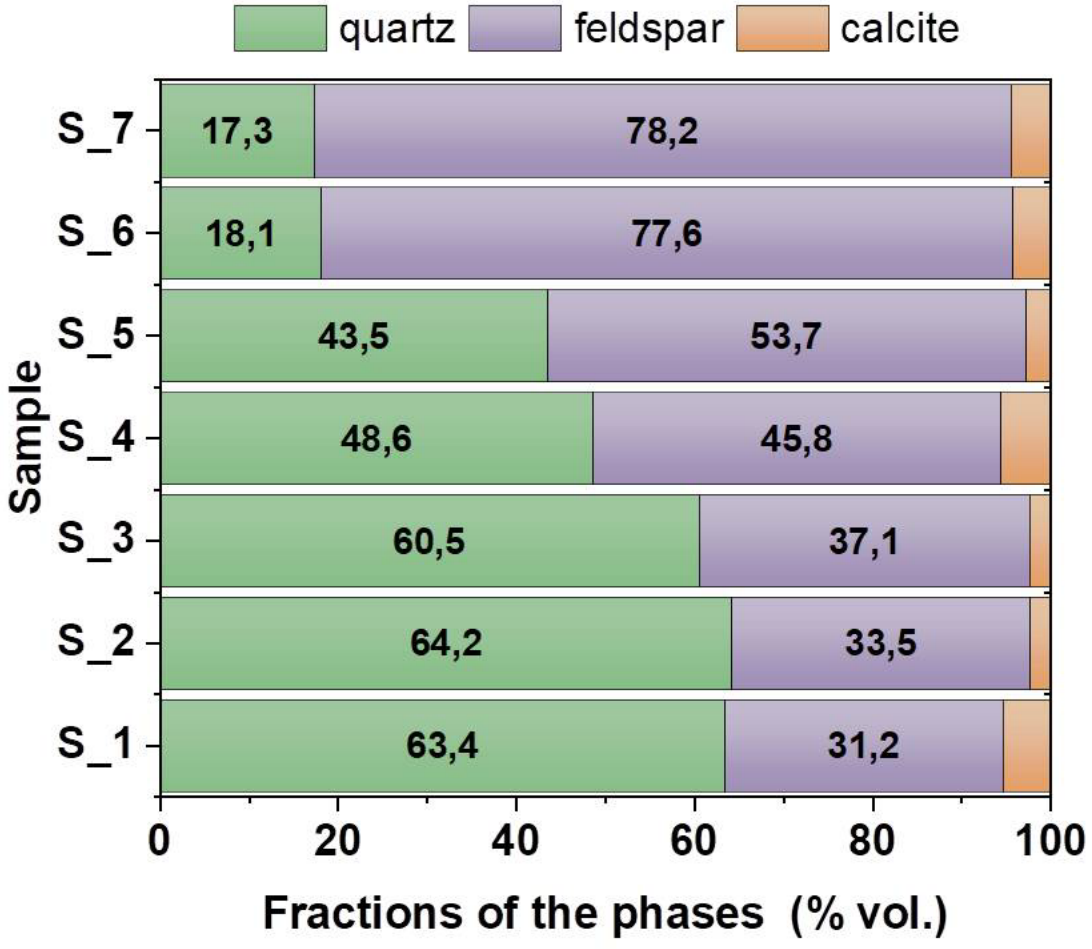

Figure 5. The diagram of the fractions of quartz, feldspar, and calcite phases after treating the neutron diffraction data by the Rietveld method.

Neutron tomography

The spatial distribution of various chemical components of ceramic products was studied using neutron radiography and tomography methods. The reconstructed

from neutron tomography data three-dimensional (3D) models of the studied ceramic fragments from the Asusay medieval settlement and the Eleke Sazy burial ground are shown in Figure 6. A fairly uniform spatial distribution of the neutron beam attenuation coefficients inside the volume of the fragment indicates the completion of the firing process during ceramic item preparation, when there is uniform oxidation in the core and surface regions [24]. Several large inclusions characterized by high neutron attenuation coefficients were found inside the volume of the ceramic fragments S_1 and S_4. We believe that the inclusions can be grains of silicate minerals [26]. The linear dimensions of these grains are in the range of 0.4 – 1.5 mm.

For the sample S_1, the larger grain diameter is 3.19(1) mm, and the total volume of all grains is 12.14(5) mm^3, or 38626 voxels out of the 4051999 voxels in the whole volume of fragment S_1. This corresponds to 0.95 % of the total volume of sample S_1. The average volume of the observed silicate grains is 1.46(5) mm^3. Also, the inner voids and small pores were detected in the reconstructed 3D data (Figure 6). The total volume of pores occupies no more than 0.5 % of the total volume of the ceramic samples.

In contrast to the S_1 sample, the S_2 has a more isotropic distribution of the neutron attenuation coefficient throughout the volume of the fragment. There are no large silicate grains in the S_2 fragment, but some small inclusions with low neutron attenuation coefficients, as well as cracks and pores of various sizes, were observed. The total volume of silicate inclusions is 8 mm^3 or about 0.43 % of the total volume of the studied fragment, and the average grain volume is 1.08(1) mm^3. The volume of voids and cracks occupied 0.23 % of the sample volume.

Table 2.
Obtained data on the component volumes of the investigated ceramic samples from the neutron three-dimensional analysis.

Sample	Total Volume, mm^3	Pores Volume, mm^3	Impurities Volume, mm^3
S_1	1274.07(8)	5.33(2)	12.14(5)
S_2	1985.54(3)	4.56(5)	8.44(9)
S_3	3223.39(8)	3.91(2)	7.44(6)
S_4	3974.63(5)	29.72(6)	3.92(8)
S_5	5604.03(8)	58.62(7)	2.28(1)
S_6	6864.01(6)	20.64(9)	3.04(6)
S_7	1514.95(9)	1.21(5)	2.36(1)

The volume of silicate grains inside the fragment S_3 is about 7 mm^3, which corresponds to 0.23 % of the total volume of the sample. On the edge of a spiral

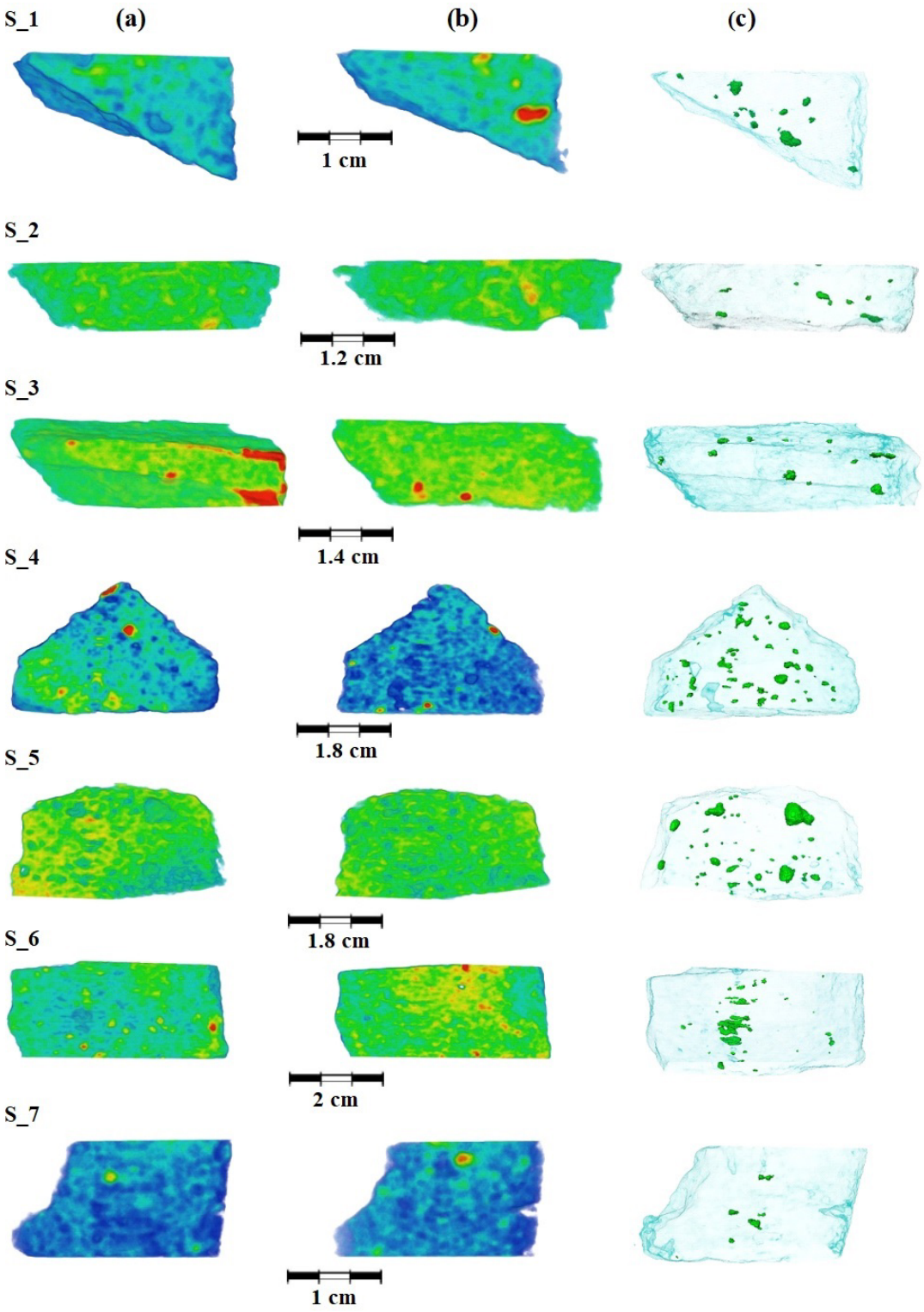

Figure 6. The 3D models (a) created after tomographic reconstruction and selected longitudinal slices (b) of the ceramic fragment. The rainbow-like coloring shows neutron absorption degrees from low (green) to high (red). The inner pores and voids are highlighted in green (c).

pattern, some regions with high neutron attenuation coefficients were found. The volume of this area is 36.75(9) mm^3, which corresponds to 1.14 % of the total volume of the jug fragment. We assume that these are remnants of contamination, probably of a soil nature. Small pores are also present in the volume of the S_3 sample. The volume of the largest pore is 1.5 mm^3.

The S_4, S_5, S_6, and S_7 ceramic fragments of the Early Iron Age period are characterized by a low content of silicate grains. Samples S_4 and S_5 demonstrate the presence of many pores of various sizes and cracks, which occupy 0.7 – 1.0 % of the total volume. The S_6 sample has a relatively homogeneous clay structure but with the presence of cracks in the central part. The part of pores and cracks is 0.03 %, while the silicate grains occupy of 0.04 % of the volume only. The smallest number of pores was found in fragment S_7.

The presence of internal pores and voids may be associated with the processes of releasing accompanying gases during the annealing of pottery objects [30]. One explanation for the difference between the size and number of internal pores is the presence of additional components in the clay material. These additional components, at high annealing temperatures, can release small amounts of carbon dioxide, which leads to the formation of inner voids. These components can be some organic materials, saline or alkaline substances, and minor phases in the clay material. In our approximation, we can say that along with the structural features of the feldspar phase, we can add the porosity factor, which can be an indirect indicator of a specific clay source for a pottery workshop.

Conclusions

For qualitative and quantitative comparative analysis of the structural features of pottery objects, we performed structural studies of two groups of ceramic fragments from various archaeological sites on the territory of the modern Republic of Kazakhstan. There are ancient medieval settlements called Asusay, which are located southwest of Akshi village in the Alakol district, and the Kagan burial complexes of Eleke Sazy. Complementary results on neutron diffraction and Raman spectroscopy and the 3D data of neutron tomography indicate a difference in the phase composition, structural features of dominant phases, and spatial arrangement of internal pores inside the ceramic fragments. This can be due to both the source of clay for the production of ceramic artifacts and the technological features of the pottery workshop.

References

[1] G. Eramo, A. Mangone, Physical Sciences Reviews **4**(11) (2019) 20180014. [*CrossRef*]
[2] L. Moraru, F. Szendrei, Journal of Engineering Studies and Research **4**(17) (2011) 73-78.
[3] M.S. Tite, Archaeometry **50**(2) (2008) 216-231. [*CrossRef*]
[4] D.P.S. Peacock, World Archaeology **1**(3) (1970) 375-389. [*CrossRef*]
[5] N. Kardjilov et al., Journal of Neutron Research **14** (2006) 29-36. [*CrossRef*]
[6] N. Kardjilov, G. Festa, Neutron Methods for Archaeology and Cultural Heritage (Springer, Cham, Switzerland, 2017) 349 p. [*CrossRef*]
[7] A.T. Toleubaev et al., Izvestiya NAS RK. Social Sciences Series **5** (2014) 154-165.

[8] N.M. Zinyakov, Bulletin of Kemerovo State University **21**(4) (2019) 932-939. [*CrossRef*] (In Russian)
[9] N.M. Zinyakov, Bulletin of Kemerovo State University **21**(3) (2019) 606-613. [*CrossRef*] (In Russian)
[10] T.N. Senigova, Srednevekovi'y Taraz (Alma-Ata: Nauka, 1972) 218 p. (In Russian)
[11] B. Lafuente et al., 1. The power of databases: The RRUFF project. (Highlights in Mineralogical Crystallography, edited by Thomas Armbruster and Rosa Micaela Danisi, Berlin, Munchen, Boston: De Gruyter (O), 2016) 30 p. [*CrossRef*]
[12] D. Kozlenko et al., Crystals **8** (2018) 331. [*CrossRef*]
[13] J. Rodriguez-Carvajal, Physica B: Condensed Matter **192** (1993) 55-69. [*CrossRef*]
[14] D.P. Kozlenko et al., Physics of Particles and Nuclei Letters **13** (2016) 346-351. [*CrossRef*]
[15] D.P. Kozlenko et al., Phys Procedia **69** (2015) 87-91. [*CrossRef*]
[16] K.M. Podurets et al., Crystallography Reports **66**(2) (2021) 254-266. [*CrossRef*]
[17] E.H. Lehmann, A.P. Kaestner, 3D Neutron Imaging (Encyclopedia of Analytical Chemistry, 2009) 17 p. [*CrossRef*]
[18] C.A. Schneider et al., Nature Methods **9** (2012) 671-675. [*CrossRef*]
[19] F. Brun et al., Advanced Structural and Chemical Imaging **3** (2017) 4. [*CrossRef*]
[20] N. Buzgar et al., J Archaeol Sci. **40**(4) (2013) 2128-2135. [*CrossRef*]
[21] J.J. Freeman et al., The Canadian Mineralogist **46**(6) (2008) 1477. [*CrossRef*]
[22] L. Medeghini et al., Journal of Raman Spectroscopy **45** (2014) 1244-1250. [*CrossRef*]
[23] D. Deldicque et al., Carbon **102** (2016) 319-329. [*CrossRef*]
[24] B.A. Bakirov et al., Eurasian Journal of Physics and Functional Materials **6** (2022) 56-70. [*CrossRef*]
[25] B. Delyon, F. Portier, Bernoulli **22**(4) (2016) 2177-2208. [*CrossRef*]
[26] L. Ghergari, C. Stancel, Studia Universitatis Babes-Bolyai, Geologia **57** (2012) 13-21. [*CrossRef*]
[27] W. Kockelmann et al., Journal of Archaeological Science **28**(2) (2001) 213-222. [*CrossRef*]
[28] I.M. Siouris, J. Walter, Physica B Condens Matter. **385-386** (2006) 225-227. [*CrossRef*]
[29] K.J. Stanienda-Pilecki, Carbonates Evaporites **33**(4) (2018) 801-821. [*CrossRef*]
[30] B.A. Abdurakhimov et al., Journal of Archaeological Science: Reports **35** (2021) 102755. [*CrossRef*]